DMD Fast Forward. Published on April 21, 2011 as doi:10.1124/dmd.111.038729

In vitro metabolism of rivoglitazone, a novel peroxisome proliferator-activated receptor γ agonist, in rat, monkey, and human liver microsomes and freshly isolated hepatocytes

Minoru Uchiyama, Hiroko Koda, Thomas Fischer, Juergen Mueller, Naotoshi Yamamura, Minoru Oguchi, Haruo Iwabuchi, Osamu Okazaki, and Takashi Izumi

Drug Metabolism and Pharmacokinetics Research Laboratories, Daiichi Sankyo Co., Ltd., Tokyo, Japan (M.U., H.K., N.Y., H.I., O.O., T.I.); Drug Metabolism Department, Daiichi Sankyo Europe GmbH., Martinsried, Germany (T.F., J.M.); and Research Department I, Daiichi Sankyo RD Associe Co., Ltd., Tokyo, Japan (M.O.)

Running Title:

In vitro metabolism of rivoglitazone

Address correspondence to:

Minoru Uchiyama

Drug Metabolism and Pharmacokinetics Research Laboratories, Daiichi Sankyo Co., Ltd., 1-2-58 Hiromachi, Shinagawa-ku, Tokyo, 140-8710, Japan

Tel: +81-3-3492-3131

Fax: +81-3-5436-8567

E-mail: uchiyama.minoru.fe@daiichisankyo.co.jp

Text Pages: 37

Table: 2

Figures: 8

References: 23

Abstract: 235 words

Introduction: 312 words

Discussion: 1491 words

Abbreviations:

rivoglitazone, (*RS*)-5-{4-[(6-methoxy-1-methyl-1*H*-benzimidazol-2-yl)methoxy]benzyl}-1,3-thiazolidine-2,4-dione monohydrochloride; TZD, thiazolidinedione; PPARγ, peroxisome

proliferator-activated receptor γ; HPLC, high-performance liquid chromatography; TFA, trifluoroacetic acid; UGT, UDP-glucuronosyltransferase; CYP, cytochrome P450; SAM, *S*-adenosyl-L-methionine; UDPGA, uridine 5'-diphosphate glucronic acid; HBSS, Hanks' balanced salt solution; radio-HPLC, radioactivity detection high-performance liquid chromatography; LC, liquid chromatography; MS, mass spectrometry; MS/MS, tandem mass spectrometry; ESI, electrospray ionization.

Abstract

The in vitro metabolism of rivoglitazone, (*RS*)-5-{4-[(6-methoxy-1-methyl-1*H*-benzimidazol-2-yl)methoxy]benzyl}-1,3-thiazolidine-2,4-dione monohydrochloride, a novel thiazolidinedione (TZD) peroxisome proliferator-activated receptor γ selective agonist, was studied in liver microsomes and freshly isolated hepatocytes of rat, monkey, and human as well as cDNA-expressed human cytochrome P450 (CYP) and UDP-glucuronosyltransferase (UGT) enzymes. Fourteen metabolites were detected and these structures were elucidated by liquid chromatography-tandem mass spectrometry. Five initial metabolic pathways of rivoglitazone consisting of four oxidation pathways and one *N*-glucuronidation pathway were predicted in correspondence with those proposed for in vivo studies using rats and monkeys. In metabolization using liver microsomes, the TZD ring-opened mercapto amide (M22) and TZD ring-opened mercapto carboxylic acid (M23) were identified as the primary metabolite of TZD ring-opening pathway and its sequential metabolite, which have not been detected previously from in vivo studies. Combination with *S*-adenosyl-L-methionine was useful to obtain the sequential *S*-methylated metabolites from the oxidative metabolites. *N*-Glucuronide and sequential TZD ring-opened metabolites were also found in liver microsomes in the presence of UDPGA. The *O*-demethyl-*O*-sulfate (M11), which is the major in vivo metabolite in rats and monkeys, was detected in all species of hepatocytes. In addition, TZD ring-opened *S*-cysteine conjugate (M15) was detected in human hepatocytes. From these results, the in vivo metabolic pathways in humans were predicted to be the four oxidation and one *N*-glucuronidation pathways. The four

DMD Fast Forward. Published on April 21, 2011 as DOI: 10.1124/dmd.111.038729
This article has not been copyedited and formatted. The final version may differ from this version.

oxidative metabolites were formed by multiple human CYP enzymes and *N*-glucuronide formed by UGT1A3 and UGT2B7, respectively.

DMD Fast Forward. Published on April 21, 2011 as DOI: 10.1124/dmd.111.038729
This article has not been copyedited and formatted. The final version may differ from this version.

Introduction

Rivoglitazone, (*RS*)-5-{4-[(6-methoxy-1-methyl-1*H*-benzimidazol-2-yl)methoxy]benzyl}-1,3-thiazolidine-2,4-dione monohydrochloride (Fig. 1), is a novel thiazolidinedione (TZD) that selectively activates the nuclear receptor peroxisome proliferator-activated receptor γ (PPARγ) (Kanda et al., 2009). TZD-containing drugs, pioglitazone and rosiglitazone, are a clinically important new class of oral antidiabetic agents for the treatment of type 2 diabetes mellitus. TZD-containing drugs increase insulin sensitivity in target tissues through interaction with the PPARγ (Sood et al., 2000). PPARγ regulates the expression of genes involved in glucose and lipid metabolism, and TZD-containing drugs are thought to exert their antidiabetic effects via the activation of PPARγ (Diamant and Heine, 2003; Semple et al., 2006).

Pharmacokinetics, metabolism, and disposition studies of rivoglitazone after oral administration of [^{14}C]rivoglitazone to rats and monkeys have been reported (Uchiyama et al., 2011). Rivoglitazone exhibits low clearance, which is mainly the result of metabolism. Twenty metabolites of rivoglitazone in rats and monkeys were identified by liquid chromatography (LC)-tandem mass spectrometry (MS/MS) using electrospray ionization (ESI). Based on the structures of the metabolites, five initial metabolic pathways consisting of four oxidation pathways and one *N*-glucuronidation pathway for rivoglitazone have been proposed: 1) *O*-demethylation to form *O*-demethyl rivoglitazone (M12); 2) TZD ring opening to form TZD ring-opened methylmercapto amide (M20) via TZD ring-opened mercapto amide (intermediate I); 3) *N*-demethylation to form *N*-demethyl rivoglitazone (M17); 4) TZD ring

hydroxylation to form TZD ring 5-hydroxy rivoglitazone (M18); and 5) *N*-glucuronidation to form *N*-glucuronide (M13).

The objective of this study was to elucidate the in vitro metabolic pathways of rivoglitazone using rat, monkey, and human liver microsomes and freshly isolated hepatocytes and then compare the pathways based on the in vivo data. Furthermore, the qualitative identification of the predominant human cytochrome P450 (CYP) and UDP-glucuronosyltransferase (UGT) enzymes for the in vitro metabolism of rivoglitazone was conducted using cDNA-expressed enzymes. Metabolite detection and identification was performed using radioactivity detection high-performance liquid chromatography (radio-HPLC), LC-mass spectrometry (MS), and LC-MS/MS.

DMD Fast Forward. Published on April 21, 2011 as DOI: 10.1124/dmd.111.038729
This article has not been copyedited and formatted. The final version may differ from this version.

Materials and Methods

Materials.

Radiolabeled [TZD-5-^{14}C]rivoglitazone (specific radioactivity, 35.4 μCi/mg; radiochemical purity, >98%) was synthesized by GE Healthcare (Little Chalfont, Buckinghamshire, UK). Rivoglitazone and the synthetic standards of its metabolites, TZD ring-opened methyl sulfoxide amide (M6), TZD ring-opened *N*-glucuronide (M9), TZD ring-opened methyl sulfone amide (M10), *O*-demethyl-*O*-sulfate (M11), *O*-demethyl rivoglitazone (M12), *N*-glucuronide (M13), TZD ring-opened *S*-cysteine conjugate (M15), *N*-demethyl rivoglitazone (M17), TZD ring 5-hydroxy rivoglitazone (M18), TZD ring-opened methylmercapto carboxylic acid (M19), TZD ring-opened methylmercapto amide (M20), TZD ring-opened mercapto amide (M22), and TZD ring-opened mercapto carboxylic acid (M23) were synthesized by Daiichi Sankyo Co., Ltd. or Daiichi Sankyo RD Associe Co., Ltd. (Tokyo, Japan). Collagenase H was purchased from Roche Diagnostics GmbH (Indianapolis, IN). Hanks' balanced salt solution (HBSS) was purchased from Mediatech (Herndon, VA). EGTA, *S*-adenosyl-L-methionine (SAM), $NADP^+$, glucose 6-phosphate, glucose-6-phosphate dehydrogenase, uridine 5'-diphosphate glucronic acid (UDPGA), and alamethicin were purchased from Sigma-Aldrich (St. Louis, MO). HEPES was purchased from Dojindo Laboratories (Kumamoto, Japan). Pooled male rat liver microsomes (prepared from 94 Sprague-Dawley rats, 20 mg/ml), pooled male monkey liver microsomes (prepared from 8 cynomolgus monkey, 20 mg/ml), and pooled human liver microsomes (prepared from 23 donors, 20 mg/ml) were purchased from BD Biosciences (Franklin Lakes, NJ). Microsomes prepared from baculovirus-infected

DMD Fast Forward. Published on April 21, 2011 as DOI: 10.1124/dmd.111.038729
This article has not been copyedited and formatted. The final version may differ from this version.

insect cells expressing human CYP1A2, CYP2C8, CYP2C9, CYP2C19, CYP2D6, CYP3A4, and CYP3A5 (Supersomes) as well as the insect cell control supersomes were purchased from BD (Woburn, MA). Microsomes prepared from baculovirus-infected insect cells expressing human UGT1A1, UGT1A3, UGT1A4, UGT1A6, UGT1A7, UGT1A8, UGT1A9, UGT1A10, UGT2B4, UGT2B7, UGT2B15, and UGT2B17 (Supersomes) as well as the UGT insect cell control supersomes were also purchased from BD Biosciences. All other reagents and solvents used were commercially available and either of analytical or high-performance liquid chromatography (HPLC) grade.

Preparation of freshly isolated human hepatocytes.

Human liver tissues from three donors were obtained from patients undergoing partial hepatectomy for metastatic liver tumors of colorectal cancer. Experimental procedures were performed according to the guidelines of the charitable state-controlled foundation Human Tissue and Cell Research (Regensburg, Germany) with informed patient's consent and approved by the local ethics committee of the University of Regensburg, Germany (Thasler et al., 2003). The liver samples were made anonymous. The human hepatocytes used were isolated and provided by Hepacult GmbH (Regensburg, Germany) after being commissioned by Human Tissue and Cell Research and Daiichi Sankyo Europe GmbH (Martinsried, Germany). Cells were isolated using a modified two-step EGTA-collagenase perfusion procedure (Weiss et al., 2003). The human hepatocytes were washed twice with HBSS and suspended in HBSS at a viable cell density of 2×10^6 cells/ml. As determined by the trypan blue dye exclusion method, the cellular viabilities of the human hepatocytes

DMD Fast Forward. Published on April 21, 2011 as DOI: 10.1124/dmd.111.038729
This article has not been copyedited and formatted. The final version may differ from this version.

were 66, 73, and 81%.

Preparation of freshly isolated rat and monkey hepatocytes.

All experimental procedures were performed in accordance with the in-house guidance of the Institutional Animal Care and Use Committee of Daiichi Sankyo Co., Ltd. (Tokyo, Japan). Freshly isolated rat and monkey hepatocytes were obtained by the standard method (Moldéus et al., 1978). The rat hepatocytes were prepared from a male Sprague-Dawley rat (Crl:CD; 7 weeks old; body weight, 170 g). The rat hepatocytes were washed twice with HBSS and suspended in HBSS at a viable cell density of 2×10^6 cells/ml. The cellular viability of the rat hepatocytes was 88%, as determined by the trypan blue dye exclusion method. The monkey hepatocytes were prepared from two male cynomolgus monkeys (*Macaca fasicularis*; 5 years old as the estimated age). The monkey hepatocytes were washed twice with HBSS and suspended in HBSS at a viable cell density of 2×10^6 cells/ml. As determined by the trypan blue dye exclusion method, the cellular viabilities of the monkey hepatocytes were 91 and 94%.

Incubation of [^{14}C]rivoglitazone with rat, monkey, and human liver microsomes in the presence of NADPH-generating system and SAM.

Incubation of [^{14}C]rivoglitazone with pooled rat, monkey, or human liver microsomes was performed as follows. The incubation mixture contained 10 mM potassium phosphate buffer (pH 7.4), NADPH-generating system (2 mM $NADP^+$, 20 mM glucose 6-phosphate, 2 units/ml glucose-6-phosphate dehydrogenase, 10 mM $MgCl_2$), 1 mg/ml microsomal protein from rat, monkey or human liver, and

[^{14}C]rivoglitazone (20 μM) at a final volume of 1 ml in the presence or absence of 2 mM SAM. The reaction mixture was incubated for 2 h at 37°C in a shaking water bath. Control incubation without NADPH-generating system and SAM alone was carried out under otherwise similar conditions. The each reaction was terminated by the addition of acetonitrile (2 ml). After centrifugation at 21,600 *g* for 5 min at 4°C (himac CF15D, Hitachi Koki Co., Ltd., Tokyo, Japan), each supernatant was carefully collected and evaporated under a nitrogen stream to an approximate final volume of 0.5 ml. Each concentrated sample was used for analysis of the metabolites by radio-HPLC, LC-MS, and LC-MS/MS.

Incubation of [^{14}C]rivoglitazone with rat, monkey, and human liver microsomes in the presence of UDPGA and SAM.

Incubation of [^{14}C]rivoglitazone with pooled rat, monkey, or human liver microsomes was performed as follows. The incubation mixture contained 100 mM Tris-HCl buffer (pH 7.5), 10 mM $MgCl_2$, 1 mg/ml microsomal protein from rat, monkey or human liver, 5 mM UDPGA, and [^{14}C]rivoglitazone (20 μM) at a final volume of 0.5 ml in the presence or absence of 2 mM SAM. Before starting incubation, the microsomes were treated with alamethicin (50 μg/mg protein) on ice for 15 min. The reaction was started by the addition of UDPGA. The reaction mixture was incubated for 4 h at 37°C in a shaking water bath. Control incubation without UDPGA and SAM alone was carried out under otherwise similar conditions. The reaction was terminated by the addition of acetonitrile (1 ml). After centrifugation at 21,600 *g* for 5 min at 4°C, the supernatant was carefully collected and evaporated under a nitrogen stream to an approximate final volume of 0.3 ml. Each

DMD Fast Forward. Published on April 21, 2011 as DOI: 10.1124/dmd.111.038729
This article has not been copyedited and formatted. The final version may differ from this version.

concentrated sample was used for analysis of the metabolites by radio-HPLC, LC-MS, and LC-MS/MS.

Incubation of [^{14}C]rivoglitazone with freshly isolated hepatocytes.

[^{14}C]Rivoglitazone (30 μM) was incubated with viable rat, monkey, or human hepatocytes suspended with HBSS (2×10^6 cells/ml) for 3 h at 37°C under 95 % O_2 and 5% CO_2 in an incubator (incubation volume, 2.5 ml each; incubation numbers for rat, $n = 1$; monkeys, $n = 2$; humans, $n = 3$, as collected in the above section). For human hepatocytes, the initial viabilities were 66 to 81%, and the remaining CYP3A4 activities (testosterone 6β-hydroxylation) after incubation for 3 h were 60 to 100% of the initial activity. For rat and monkey hepatocytes, the initial viabilities were 88% and 91 to 94%, respectively. The reactions were terminated by the addition of acetonitrile (5 ml). The cells were homogenized by sonication and samples of the incubated hepatocytes were stored at approximately –80°C until use. For each species (rat, monkeys, or humans), the samples were pooled and centrifuged at 21,600 *g* for 5 min at 4°C, and each supernatant was carefully collected. Each supernatant was evaporated under a nitrogen stream to an approximate final volume of 1.5 ml. Each concentrated sample was used for analysis of the metabolites by radio-HPLC, LC-MS, and LC-MS/MS.

Incubation of [^{14}C]rivoglitazone with cDNA-expressed human CYP enzymes in the presence of NADPH-generating system.

The incubation mixture contained 50 mM potassium phosphate buffer (pH 7.4) or 100 mM Tris-HCl buffer (pH 7.5), NADPH-generating system (2 mM $NADP^+$, 20 mM

DMD Fast Forward. Published on April 21, 2011 as DOI: 10.1124/dmd.111.038729
This article has not been copyedited and formatted. The final version may differ from this version.

glucose 6-phosphate, 2 units/ml glucose-6-phosphate dehydrogenase, 10 mM $MgCl_2$), 1 mg/ml microsomal protein from CYP1A2, CYP2C8, CYP2C9, CYP2C19, CYP2D6, CYP3A4, or CYP3A5, and [^{14}C]rivoglitazone (20 μM) at a final volume of 0.5 ml. The reaction mixture was incubated for 2 h at 37°C in a shaking water bath. Control incubation with NADPH-generating system and insect cell control supersomes was carried out under otherwise similar conditions. The reaction was terminated by the addition of acetonitrile (1 ml). After centrifugation at 21,600 *g* for 5 min at 4°C, the supernatant was carefully collected and concentrated under a nitrogen stream to an approximate final volume of 0.3 ml. Each concentrated sample was used for analysis of the metabolites by radio-HPLC, LC-MS, and LC-MS/MS.

Incubation of [^{14}C]rivoglitazone with cDNA-expressed human UGT enzymes in the presence of UDPGA.

The incubation mixture contained 100 mM Tris-HCl buffer (pH 7.5), 10 mM $MgCl_2$, 5 mM UDPGA, 1 mg/ml microsomal protein from UGT1A1, UGT1A3, UGT1A4, UGT1A6, UGT1A7, UGT1A8, UGT1A9, UGT1A10, UGT2B4, UGT2B7, UGT2B15, or UGT2B17, and [^{14}C]rivoglitazone (20 μM) at a final volume of 0.5 ml. Before starting incubation, the microsomes were treated with alamethicin (50 μg/mg protein) on ice for 15 min. The reaction was started by the addition of UDPGA. The reaction mixture was incubated for 4 h at 37°C in a shaking water bath. Control incubation with UDPGA and UGT insect cell control supersomes was carried out under otherwise similar conditions. The reaction was terminated by the addition of acetonitrile (1 ml). After centrifugation at 21,600 *g* for 5 min at 4°C, the supernatant was carefully collected and concentrated under a nitrogen stream to an approximate

final volume of 0.3 ml. Each concentrated sample was used for analysis of the metabolites by radio-HPLC, LC-MS, and LC-MS/MS.

Radio-HPLC.

Samples from all incubations were analyzed by radio-HPLC. The radio-HPLC was conducted using an L-6000 HPLC system (Hitachi, Ltd., Tokyo, Japan) combined with a Radiomatic 525TR radioactivity detector (PerkinElmer Life and Analytical Sciences, Waltham, MA). Chromatographic separation was performed on a YMC-Pack ODS-A column (6.0 × 150 mm, 5 μm; YMC Co., Ltd., Kyoto, Japan) at ambient temperature. The mobile phase, consisting of water containing 0.01% trifluoroacetic acid (TFA) (solvent A) and acetonitrile containing 0.01% TFA (solvent B), was delivered at a flow rate of 1 ml/min. The gradient started at 12% solvent B, increased linearly to 60% solvent B for 30 min, increased linearly to 90% solvent B for 5 min, and then was held at 90% solvent B for 5 min. The column effluent was monitored using an L-4000 UV detector (UV at 220 nm; Hitachi, Ltd.) and a radioactivity detector with a 3 ml/min flow rate for the Ultima-Flo M liquid scintillator (PerkinElmer Life and Analytical Sciences).

LC-MS and LC-MS/MS.

The conditions described below were used for the LC-MS and LC-MS/MS of the rivoglitazone metabolites. These analyses were performed using a quadrupole time-of-flight mass spectrometer (Waters, Manchester, UK) with an L-7000 HPLC system (Hitachi, Ltd.) consisting of an intelligent pump (model L-7100), a column oven (model L-7300), a chromatointegrator (model D-7500), and a UV detector (model

L-7400S). The LC-MS was conducted using ESI in the positive ion mode. The capillary voltage and cone voltage were set at 3300 and 45 V, respectively. The source temperature and desolvation gas temperature were 120 and 300°C, respectively. The mass range from *m/z* 50 to 1000 was acquired with an integration time of 1 s. The LC-MS/MS was performed using a collision energy of 20 eV and xenon as the collision gas. Chromatographic separation was performed on a YMC-Pack ODS-A column (1.5 × 150 mm, 5 μm; YMC Co., Ltd.). The column temperature was maintained at 30°C, and UV detection was at 220 nm. The mobile phase consisted of water containing 0.01% TFA (solvent A) and acetonitrile containing 0.01% TFA (solvent B). The gradient started at 12% solvent B, increased linearly to 60% solvent B for 30 min, increased linearly to 90% solvent B for 5 min, and then was held at 90% solvent B for 5 min. The flow rate was set at 0.1 ml/min, and the elution flow from the HPLC system was introduced into the quadrupole time-of-flight mass spectrometer ionization source through an ESI interface.

DMD Fast Forward. Published on April 21, 2011 as DOI: 10.1124/dmd.111.038729
This article has not been copyedited and formatted. The final version may differ from this version.

Results

Metabolism of rivoglitazone in rat, monkey, and human liver microsomes in the presence of NADPH-generating system and SAM.

After incubation of [^{14}C]rivoglitazone with liver microsomes in the presence of NADPH-generating system alone yielded qualitatively similar metabolic profiles in rat, monkey, and human liver microsomes (Fig. 2, a–c; Table 1). Three oxidative metabolites formed in these incubations, *O*-demethyl rivoglitazone (M12), *N*-demethyl rivoglitazone (M17), and TZD ring 5-hydroxy rivoglitazone (M18), and were identified by comparison of their HPLC retention times and LC-MS/MS spectra with those of synthetic standards (Table 2), including those that have been identified previously by in vivo studies in rats and monkeys (Uchiyama et al., 2011). Moreover, three novel metabolites, that have not been identified before, TZD ring-opened hydroxy amide (M21), TZD ring-opened mercapto amide (M22), and TZD ring-opened mercapto carboxylic acid (M23), were also elucidated by LC-MS/MS (Table 2). Formation of these metabolites was NADPH-dependent. In the presence of both the NADPH-generating system and SAM, four additional *S*-methylated metabolites, TZD ring-opened methylmercapto amide (M20), TZD ring-opened methyl sulfoxide amide (M6), TZD ring-opened methyl sulfone amide (M10), and TZD ring-opened methylmercapto carboxylic acid (M19), were also identified (Fig. 2, d–f; Table 2).

Metabolism of rivoglitazone in rat, monkey, and human liver microsomes in the presence of UDPGA and SAM.

DMD Fast Forward. Published on April 21, 2011 as DOI: 10.1124/dmd.111.038729
This article has not been copyedited and formatted. The final version may differ from this version.

After incubation of [^{14}C]rivoglitazone with liver microsomes in the presence of UDPGA, qualitatively similar metabolic profiles were observed in rat, monkey, and human liver microsomes (Fig. 3, a–c; Table 1). Three metabolites formed in these incubations, *N*-glucuronide (M13), TZD ring-opened *N*-glucuronide (M9), and TZD ring-opened mercapto carboxylic acid (M23), and were identified by comparison of their HPLC retention times and LC-MS/MS spectra with those of synthetic standards (Table 2). Moreover, in the presence of both UDPGA and SAM, an additional *S*-methylated metabolite of M23, TZD ring-opened methylmercapto carboxylic acid (M19), was detected (Fig. 3, d–f; Table 2).

Metabolism of [^{14}C]rivoglitazone in freshly isolated rat, monkey, and human hepatocytes.

Representative radiochromatograms after incubation of [^{14}C]rivoglitazone with freshly isolated rat, monkey, and human hepatocytes are shown in Fig. 4. Ten metabolites, M6, M9, M10, M12, M13, M17, M18, and M20, including two phase II conjugated metabolites *O*-demethyl-*O*-sulfate (M11) and TZD ring-opened *S*-cysteine conjugate (M15), were detected in human hepatocytes (Tables 1 and 2). M11 and M15 were not detected in liver microsomal incubations. In rat hepatocytes, nine metabolites, M6, M9, M10, M11, M12, M13, M17, M18, and M20, were also detected, but M15 was not detected (Table 1). In monkey hepatocyes, six metabolites, M9, M11, M12, M13, M18, and M20, were also detected, but M6, M10, M15, and M17 were not detected (Table 1). Thus, M15 was a unique human metabolite in hepatocytes.

DMD Fast Forward. Published on April 21, 2011 as DOI: 10.1124/dmd.111.038729
This article has not been copyedited and formatted. The final version may differ from this version.

Metabolism of [^{14}C]rivoglitazone with cDNA-expressed human CYP enzymes in the presence of NADPH-generating system.

After incubation of [^{14}C]rivoglitazone with cDNA-expressed human CYP1A2, CYP2C8, CYP2C9, CYP2C19, CYP2D6, CYP3A4, and CYP3A5 in the presence of NADPH-generating system, four metabolites, M12, M17, M18, and M22, were formed by these CYP enzymes (Table 1). In addition, sequential metabolites M21 and M23 were also detected (Table 1).

Incubation of [^{14}C]rivoglitazone with cDNA-expressed human UGT enzymes in the presence of UDPGA.

After incubation of [^{14}C]rivoglitazone with cDNA-expressed human UGT1A1, UGT1A3, UGT1A4, UGT1A6, UGT1A7, UGT1A8, UGT1A9, UGT1A10, UGT2B4, UGT2B7, UGT2B15, and UGT2B17 in the presence of UDPGA, two *N*-glucuronide metabolites, M13 and M9, were formed by UGT1A3 and UGT2B7 (Table 1). In addition, sequential metabolite M23 was observed at a trace level (Table 1). However, in UGT1A1, UGT1A4, UGT1A6, UGT1A7, UGT1A8, UGT1A9, UGT1A10, UGT2B4, UGT2B15, and UGT2B17, M13, M9, and M23 were not detected (data not shown).

Identification of rivoglitazone metabolites by LC-MS/MS

The structures of the 14 metabolites were identified by LC-MS/MS (Table 2). The 11 metabolites M6, M9 to M13, M15, and M17 to M20 were further identified by comparing their mass spectra and retention times on HPLC with those of synthetic standards (Uchiyama et al., 2011). Similarly, the novel metabolites M23 and M22

DMD Fast Forward. Published on April 21, 2011 as DOI: 10.1124/dmd.111.038729
This article has not been copyedited and formatted. The final version may differ from this version.

were also identified by comparing with those of synthetic standards (Supplemental Figs. S1 and S2).

Structure analysis of M21.

The positive ion LC-MS spectrum of M21 showed a protonated molecule $[M + H]^+$ at *m/z* 356. The LC-MS/MS spectrum of M21, which was obtained by collision-induced dissociation of the ion $[M + H]^+$ at *m/z* 356, and the proposed fragmentation scheme are shown in Fig. 5. Product ions at *m/z* 161, 176, 282, and 311 were obtained. The most intense product ion at *m/z* 176 formed via the loss of 180 Da from the ion $[M + H]^+$ at *m/z* 356. The product ions at *m/z* 161 and 176 indicated that the 6-methoxy-1-methyl-benzimidazole moiety was not metabolized. The product ion at *m/z* 311 was formed via the elimination of the carbamoyl group from the ion $[M + H]^+$ at *m/z* 356. The product ion at *m/z* 282 was formed via the elimination of the hydroxyl and carbamoyl groups from the ion $[M + H]^+$ at *m/z* 356. Based on these results, M21 was proposed to be a TZD ring-opened hydroxy amide (Table 2).

Structure analysis of M22.

The positive ion LC-MS spectrum of M22 showed a protonated molecule $[M + H]^+$ at *m/z* 372. The LC-MS/MS spectrum of the precursor ion $[M + H]^+$ at *m/z* 372 and the proposed fragmentation scheme of M22 are shown in Fig. 6. Product ions at *m/z* 161, 176, 268, 282, 294, and 327 were obtained. The most intense product ion at *m/z* 176 formed via the loss of 196 Da from the ion $[M + H]^+$ at *m/z* 372 indicated that the 6-methoxy-1-methyl-benzimidazole moiety was not modified. The product ion at

DMD Fast Forward. Published on April 21, 2011 as DOI: 10.1124/dmd.111.038729
This article has not been copyedited and formatted. The final version may differ from this version.

m/z 327 was formed via the elimination of the carbamoyl group from the ion $[M + H]^+$ at *m/z* 372. The product ion at *m/z* 294 was formed via the elimination of the mercapto and carbamoyl groups from the ion $[M + H]^+$ at *m/z* 372. Furthermore, the LC-MS/MS spectrum and HPLC retention time of M22 were identical to those of the synthetic standard. Based on these results, M22 was identified as a TZD ring-opened mercapto amide (Table 2).

Structure analysis of M23.

The positive ion LC-MS spectrum of M23 showed a protonated molecule $[M + H]^+$ at *m/z* 373, which was 1 Da higher than that of M22. The LC-MS/MS spectrum of the precursor ion $[M + H]^+$ at *m/z* 373 and the proposed fragmentation scheme of M23 are shown in Fig. 7. Similar to M22, product ions at *m/z* 161, 176, 268, 282, 295, and 327 were obtained. The most intense product ion at *m/z* 176 formed via the loss of 197 Da from the ion $[M + H]^+$ at *m/z* 373 indicated that the 6-methoxy-1-methyl-benzimidazole moiety was not metabolized. The product ion at *m/z* 327 was formed via the elimination of the carboxylic acid group from the ion $[M + H]^+$ at *m/z* 373. The product ion at *m/z* 295 was formed via the elimination of the mercapto and carboxylic acid groups from the ion $[M + H]^+$ at *m/z* 373. Furthermore, the LC-MS/MS spectrum and HPLC retention time of M23 were identical to those of the synthetic standard. Based on these results, M23 was identified as a TZD ring-opened mercapto carboxylic acid (Table 2).

DMD Fast Forward. Published on April 21, 2011 as DOI: 10.1124/dmd.111.038729
This article has not been copyedited and formatted. The final version may differ from this version.

Discussion

The present evaluation of the in vitrol metabolism of rivoglitazone in rat, monkey, and human liver microsomes and hepatocytes led to the identification of 14 metabolites by LC-MS/MS. Rats and monkeys used for toxicity and pharmacology testing of rivoglitazone were used for these metabolism studies. The objective of this study was to elucidate the in vitro metabolic pathways of rivoglitazone (Fig. 8) and compare the pathways with in vivo data (Uchiyama et al., 2011).

After incubation of [^{14}C]rivoglitazone with liver microsomes in the presence of NADPH-generating system, 6 metabolites were detected in all species. Four oxidative metabolites were detected: *O*-demethyl rivoglitazone (M12), *N*-demethyl rivoglitazone (M17), TZD ring 5-hydroxy rivoglitazone (M18), and TZD ring-opened mercapto amide (M22). These metabolites correspond to the proposed primary oxidative metabolic pathways of rivoglitazone in vivo study: *O*-demethylation, *N*-demethylation, TZD ring hydroxylation, and TZD ring opening, respectively. In particular, M22 was not detected in in vivo study in rats and monkeys, but was speculated as intermediate I based on the structure of TZD ring-opened methylmercapto amide (M20). In addition, TZD ring-opened mercapto carboxylic acid (M23) was also identified, which was estimated as intermediate II to be metabolized from M22 in in vivo study. In this study, we could confirm the chemical structure of M22 as the primary metabolite for TZD ring-opening pathway and M23 as its sequential metabolite. Furthermore, after incubation with liver microsomes in the presence of both NADPH-generating system and SAM, M22 was metabolized to TZD ring-opened methyl sulfone amide (M10) via M20 and its sequential oxidative metabolite, TZD ring-opened methyl sulfoxide amide

DMD Fast Forward. Published on April 21, 2011 as DOI: 10.1124/dmd.111.038729
This article has not been copyedited and formatted. The final version may differ from this version.

(M6) by *S*-methylation and further oxidation. M22 was also metabolized via M23 to TZD ring-opened methylmercapto carboxylic acid (M19). These metabolites after incubation with liver microsomes in the presence of NADPH-generating system and SAM were observed in in vivo study. Thus, the combination system of NADPH-generating system and SAM was useful to obtain metabolites related to oxidation and sequential *S*-methylation and accurately reflected the metabolite profiles of rivoglitazone in vivo.

After incubation with liver microsomes in the presence of UDPGA, *N*-glucuronide (M13), TZD ring-opened *N*-glucuronide (M9), and M23 were formed. M9 was thought to be formed by nonenzymatic hydrolysis from M13 (Uchiyama et al., 2011). The chemical mechanism of the ring opening of TZD ring of rivoglitazone is unknown. However, after *N*-glucuronidation of the TZD ring, the formation of hydrogen bonding between the hydroxyl group at 2-position of the glucuronic acid moiety and the carbonyl group at 4-position of the TZD ring would be proposed. As a result, the increase of the electrophilicity of the TZD ring may be easily attacked by a nucleophile and sequentially hydrolyzed. In addition, if the chemical reactivity of M13 is very high, there may be the possibility of detecting glutathione conjugates, but no glutathione conjugates were observed in this study.

Interestingly, M23 was formed via two different pathways: oxidative TZD ring-opening pathway (hydrolysis of carbamoyl group of M22) and *N*-glucuronidation pathway (cleavage of *S*-carbamoyl moiety of M9). However, we have found that the formation of M23 from *N*-glucuronidation pathway is more common than that from oxidative TZD ring-opening pathway based on the in vitro study using synthetic standards of M9 and M22 (Uchiyama et al., 2011).

From in vitro and in vivo study of rivoglitazone in rats and monkeys, we have reported two types of TZD ring-opening pathways: oxidative pathway and intermediate *N*-glucuronidation pathway. For an oxidative pathway, the cleavage of S-C bond between 1-position and 2-position of the TZD ring formed M22 via sulfoxide intermediate. This oxidative TZD ring-opening pathway of troglitazone has been considered to be related to hepatotoxicity (Kassahun et al., 2001; Smith, 2003). However, pioglitazone and rosiglitazone, which have been observed as similar to oxidative TZD ring-opening pathways (Baughman et al., 2005; Uchiyama et al., 2010a; Uchiyama et al., 2010b), have not caused serious hepatotoxicity. One of the reasons for the difference may be due to that of daily doses: troglitazone, 400–600 mg; piogiltazone, 15–45 mg; and rosiglitazone, 4–8 mg (Nakayama et al., 2009; Usui et al., 2009). The efficacy of rivoglitazone have been observed at less than 5 mg/day in the clinical study (Rohatagi et al., 2008). For intermediate *N*-glucuronidation pathway, the cleavage of N-C bond between 3-position and 4-position of TZD ring by hydrolysis formed M23 via M9. The similar dual TZD ring-opening pathways have been observed for pioglitazone (Uchiyama et al., 2010a) and rosiglitazone (Uchiyama et al., 2010b). However, the contribution of *N*-glucuronidation, which was present in both drugs and observed in the in vitro study using hepatocytes, did not occur in the in vivo study. While, the contribution of the in vivo *N*-glucuronidation pathway of rivoglitazone was predicted to be 3.3 to 4.7% for rats and 13% for monkeys (Uchiyama et al., 2011). Thus, the contribution of intermediate *N*-glucuronidation to TZD ring opening of rivoglitazone was estimated to be high compared to pioglitazone and rosiglitazone.

After incubation with freshly isolated rat, monkey, and human hepatocytes, 9, 6,

and 10 metabolites were detected, respectively. Primary or secondary metabolites involving five metabolic pathways have been observed in rat and human hepatocytes, but four metabolic pathways were observed in monkeys with the exclusion of the *N*-demethylation pathway. On the other hand, we have observed the formation of M17 in monkey liver microsomes, plasma and bile after oral dosing of [^{14}C]rivoglitazone. The reasons for the difference are not known at this time.

The primary metabolite for TZD ring-opening pathway, M22, was not observed, but the sequential metabolite M20 was observed in all species. In addition, the sequential metabolites from M20, M6 and M10 were formed in rat and human hepatocytes. This suggests that oxidation and sequential *S*-methylation system have contributed to the metabolism of rivoglitazone in hepatocytes.

O-Demethyl-*O*-sulfate (M11) is the sequential metabolite of M12, which is responsible for the major metabolic pathway in rats and monkeys and was formed in all species of hepatocytes. M11 is thought to be a sulfate of M12. Similar metabolic pathways of oxidative *O*-demethylation and sequential *O*-sulfation were observed for apixaban. *O*-Demethyl apixaban sulfate was detected in in vivo as a major metabolite in animals and human and also in vitro major metabolite in hepatocytes (Zhang et al., 2009).

In addition, TZD ring-opened *S*-cysteine conjugate (M15), which has been observed in monkey plasma as a minor metabolite (Uchiyama et al., 2011), was observed in human hepatocytes. There are thought to be two formation pathways of M15: sequential metabolism from glutathione conjugate via cysteinyl glycine conjugate of M23 or non-glutathione mediated cysteine conjugation. The non-glutathione mediated cysteine conjugation pathway was also reported for

prasugrel (Smith et al., 2007; Farid et al., 2007) while the pathway via glutathione conjugate in hepatocytes was reported for para-aminophenol (Yan et al., 2000) and brevetoxin (Radwan and Ramsdell, 2006). For rivoglitazone, the nonenzymatic transformation of M23 to M15 was observed in buffer solution (pH 7.4) during incubation with M23 (synthetic standard) and cysteine at 37°C (data not shown). Additionally, the *S*-glutathione conjugate or sequential cysteinyl glycine conjugate of M23 was not observed in in vitro or in vivo studies. Therefore, the formation pathway of M15 was speculated as a non-glutathione mediated cysteine conjugation pathway. Thus, the in vitro metabolism study of rivoglitazone using hepatocytes has provided us the useful information about in vivo metabolites such as M11 and M15.

The metabolic pathways proposed from the in vitro study using liver microsomes and hepatocytes in rat and monkey accurately reflected those based on in vivo metabolic pathways. Therefore, the in vivo metabolic pathways in human studies are also speculated to involve the four oxidation pathways and one *N*-glucuronidation pathway. The U.S. Food and Drug Administration (Guidance for Industry: Metabolites in Safety Testing, 2008, http://www.fda.gov/cder/guidance) and International Conference on Harminisation (Guidance on nonclinical safety studies for the conduct of human clinical trials and marketing authorization for pharmaceuticals, 2009, http://www.ich.org/LOB/media/MEDIA5544.pdf.) have recently issued a formal guidance on the safety testing of drug metabolites. To address the above guidances, the in vitro study using human tissues (Dalvie et al., 2009) and the comparison between in vivo and in vitro study in animals (Yu et al., 2010) will be useful information to predict the human metabolite profiles in vivo.

Qualitative identification using cDNA-expressed CYPs and UGTs suggested that

the four oxidative pathways will be contributed by multiple CYP enzymes and *N*-glucuronidation pathway will be contributed by UGT1A3 and UGT2B7, respectively, but a detailed quantitative contribution will be necessary for enzyme kinetic study and inhibition by a specific antibody and inhibitor for each CYP and UGT.

In conclusion, five initial metabolic pathways involving four oxidation pathways and one *N*-glucuronidation pathway were observed in all species. These metabolic pathways were consistent with those observed in vivo following administration of rivoglitazone in rats and monkeys. Based on these data, the metabolic pathways of rivoglitazone in human were predicted to be similar to those of animals. In addition, rivoglitazone was predicted to be metabolized by mulitple CYP-mediated oxidation and two UGT-mediated *N*-glucuronidation, sequential several conjugation and further oxidation.

DMD Fast Forward. Published on April 21, 2011 as DOI: 10.1124/dmd.111.038729
This article has not been copyedited and formatted. The final version may differ from this version.

Acknowledgements

We thank Dr. Hideyuki Shiozawa, Drug Metabolism and pharmacokinetics Research Laboratories, Daiichi Sankyo Co., Ltd., for his careful reading of the document and scientific expertise.

DMD Fast Forward. Published on April 21, 2011 as DOI: 10.1124/dmd.111.038729
This article has not been copyedited and formatted. The final version may differ from this version.

Authorship Contributions

Participated in research design: Uchiyama, Okazaki, and Izumi.

Conducted experiments: Uchiyama, Koda, Fischer, Mueller, and Yamamura.

Contributed new reagents or analytic tools: Oguchi.

Performed data analysis: Uchiyama and Iwabuchi.

Wrote or contributed to the writing of the manuscript: Uchiyama and Izumi.

Other: not applicable.

References

Baughman TM, Graham RA, Wells-Knecht K, Silver IS, Tyler LO, Wells-Knecht M, and Zhao Z (2005) Metabolic activation of pioglitazone identified from rat and human liver microsomes and freshly isolated hepatocytes. *Drug Metab Dispos* **33:**733-738.

Dalvie D, Obach RS, Kang P, Prakash C, Loi CM, Hurst S, Nedderman A, Goulet L, Smith E, Bu HZ, and Smith DA (2009) Assessment of three human in vitro systems in the generation of major human excretory and circulating metabolites. *Chem Res Toxicol* **22:**357-368.

Diamant M and Heine RJ (2003) Thiazolidinediones in type 2 diabetes mellitus: current clinical evidence. *Drugs* **63:**1373-1405.

Farid NA, Smith RL, Gillespie TA, Rash TJ, Blair PE, Kurihara A, and Goldberg MJ (2007) The disposition of prasugrel, a novel thienopyridine, in humans. *Drug Metab Dispos* **35:**1096-1104.

Kanda S, Nakashima R, Takahashi K, Tanaka J, Ogawa J, Ogata T, Yachi M, Araki K, and Ohsumi J (2009) Potent antidiabetic effects of rivoglitazone, a novel peroxisome proliferator-activated receptor-γ agonist, in obese diabetic rodent models. *J Pharmacol Sci* **111:**155-166.

Kassahun K, Pearson PG, Tang W, McIntosh I, Leung K, Elmore C, Dean D, Wang R,

Doss G, and Baillie TA (2001) Studies on the metabolism of troglitazone to reactive intermediates in vitro and in vivo. Evidence for novel biotransformation pathways involving quinone methide formation and thiazolidinedione ring scission. *Chem Res Toxicol* **14:**62-70.

Moldéus P, Högberg J, and Orrenius S (1978) Isolation and use of liver cells. *Methods Enzymol* **52:**60-71.

Nakayama S, Atsumi R, Takakusa H, Kobayashi Y, Kurihara A, Nagai Y, Nakai D, and Okazaki O (2009) A zone classification system for risk assessment of idiosyncratic drug toxicity using daily dose and covalent binding. *Drug Metab Dispos* **37:**1970-1977.

Radwan FF and Ramsdell JS (2006) Characterization of in vitro oxidative and conjugative metabolic pathways for brevetoxin (PbTx-2). *Toxicol Sci* **89:**57-65.

Rohatagi S, Carrothers TJ, Jin J, Jusko WJ, Khariton T, Walker J, Truitt K, and Salazar DE (2008) Model-based development of a PPARγ agonist, rivoglitazone, to aid dose selection and optimize clinical trial designs. *J Clin Pharmacol* **48:**1420-1429.

Semple RK, Chatterjee VK, and O'Rahilly S (2006) PPARγ and human metabolic disease. *J Clin Invest* **116:**581-589.

Smith MT (2003) Mechanisms of troglitazone hepatotoxicity. *Chem Res Toxicol* **16:**679-687.

Smith RL, Gillespie TA, Rash TJ, Kurihara A, and Farid NA (2007) Disposition and metabolic fate of prasugrel in mice, rats, and dogs. *Xenobiotica* **37:**884-901.

Sood V, Colleran K, and Burge MR (2000) Thiazolidinediones: a comparative review of approved uses. *Diabetes Technol Ther* **2:**429-440.

Thasler WE, Weiss TS, Schillhorn K, Stoll PT, Irrgang B, and Jauch KW (2003) Charitable state-controlled foundation human tissue and cell research: ethic and legal aspects in the supply of surgically removed human tissue for research in the academic and commercial sector in germany. *Cell Tissue Bank* **4:**49-56.

Uchiyama M, Fischer T, Mueller J, Oguchi M, Yamamura N, Koda H, Iwabuchi H, and Izumi T (2010a) Identification of novel metabolic pathways of pioglitazone in hepatocytes: *N*-glucuronidation of thiazolidinedione ring and sequential ring-opening pathway. *Drug Metab Dispos* **38:**946-956.

Uchiyama M, Iwabuchi H, Tsuruta F, Abe K, Takahashi M, Koda H, Oguchi M, Okazaki O, and Izumi T (2011) Pharmacokinetics, metabolism, and disposition of rivoglitazone, a novel peroxisome proliferator-activated receptor γ agonist, in rats and monkeys. *Drug Metab Dispos* **39:**653-666.

Uchiyama M, Oguchi M, Yamamura N, Koda H, Fischer T, Mueller J, Izumi T, and Iwabuchi H (2010b) Identification of novel metabolites of rosiglitazone in freshly

isolated human, rat, and monkey hepatocytes by liquid chromatography/tandem mass spectrometry. *J Mass Spectrom Soc Jpn* **58:**1-11.

Usui T, Mise M, Hashizume T, Yabuki M, and Komuro S (2009) Evaluation of the potential for drug-induced liver injury based on in vitro covalent binding to human liver proteins. *Drug Metab Dispos* **37:**2383-2392.

Weiss TS, Pahernik S, Scheruebl I, Jauch KW, and Thasler WE (2003) Cellular damage to human hepatocytes through repeated application of 5-aminolevulinic acid. *J Hepatol* **38:**476-482.

Yan Z, Nikelly JG, Killmer L Jr, and Tarloff JB (2000) Metabolism of para-aminophenol by rat hepatocytes. *Drug Metab Dispos* **28:**880-886.

Yu H, Bischoff D, and Tweedie D (2010) Challenges and solutions to metabolites in safety testing: impact of the international conference on harmonization M3(R2) guidance. *Expert Opin Drug Metabo Toxicol* **6:**1539-1549.

Zhang D, He K, Raghavan N, Wang L, Mitroka J, Maxwell BD, Knabb RM, Frost C, Schuster A, Hao F, Gu Z, Humphreys WG, and Grossman SJ (2009) Comparative metabolites of 14C-labeled apixaban in mice, rats, rabbits, dogs, and humans. *Drug Metab Dispos* **37:**1738-1748.

DMD Fast Forward. Published on April 21, 2011 as DOI: 10.1124/dmd.111.038729
This article has not been copyedited and formatted. The final version may differ from this version.

Footnotes

Address correspondence to:

Minoru Uchiyama

Drug Metabolism and Pharmacokinetics Research Laboratories, Daiichi Sankyo Co., Ltd., 1-2-58, Hiromachi, Shinagawa-ku, Tokyo 140-8710, Japan.

Tel: +81-3-3492-3131

Fax: +81-3-5436-8567

E-mail: uchiyama.minoru.fe@daiichisankyo.co.jp

DMD Fast Forward. Published on April 21, 2011 as DOI: 10.1124/dmd.111.038729
This article has not been copyedited and formatted. The final version may differ from this version.

Figure Legends

Fig. 1 Chemical structure of [^{14}C]rivoglitazone. *, indicates position of ^{14}C label.

Fig. 2 Representative radiochromatograms after incubation of [^{14}C]rivoglitazone (20 μM) with liver microsomes for 2 h at 37°C. [^{14}C]rivoglitazone was incubated with rat (a), monkey (b), and human (c) liver microsomes in the presence of NADPH-generating system. [^{14}C]rivoglitazone was incubated with rat (d), monkey (e), and human (f) liver microsomes in the presence of NADPH-generating system and SAM.

Fig. 3 Representative radiochromatograms after incubation of [^{14}C]rivoglitazone (20 μM) with liver microsomes for 4 h at 37°C. [^{14}C]rivoglitazone was incubated with rat (a), monkey (b), and human (c) liver microsomes in the presence of UDPGA. [^{14}C]rivoglitazone was incubated with rat (d), monkey (e), and human (f) in the presence of UDPGA and SAM.

Fig. 4 Representative radiochromatograms after incubation of [^{14}C]rivoglitazone (30 μM) with freshly isolated rat (a), monkey (b), and human (c) hepatocytes for 3 h at 37°C.

Fig. 5 LC-MS/MS spectrum of the ion $[M + H]^+$ at *m/z* 356 and the proposed fragmentation scheme of M21.

DMD Fast Forward. Published on April 21, 2011 as DOI: 10.1124/dmd.111.038729
This article has not been copyedited and formatted. The final version may differ from this version.

Fig. 6 LC-MS/MS spectrum of the ion $[M + H]^+$ at *m/z* 372 and the proposed fragmentation scheme of M22.

Fig. 7 LC-MS/MS spectrum of the ion $[M + H]^+$ at *m/z* 373 and the proposed fragmentation scheme of M23.

Fig. 8 Proposed in vitro metabolic pathways of rivoglitazone in rat, monkey, and human.

DMD Fast Forward. Published on April 21, 2011 as DOI: 10.1124/dmd.111.038729
This article has not been copyedited and formatted. The final version may differ from this version.

Table 1 Detection of rivoglitazone metabolites in incubations with liver microsomes, freshly isolated hepatocytes, and cDNA-expressed human CYP and UGT isoforms.

Metabolite	Occurrence														
	RLM	MLM	HLM	RH	MH	HH	CYP1A2	CYP2C8	CYP2C9	CYP2C19	CYP2D6	CYP3A4	CYP3A5	UGT1A3	UGT2B7
M6[b]	+	+	+	+	–	+	–	–	–	–	–	–	–	–	–
M9[c, d]	+	+	+	+	+	+	–	–	–	–	–	–	–	+	+
M10[b]	+	+	+	+	–	+	–	–	–	–	–	–	–	–	–
M11	–	–	–	+	+	+	–	–	–	–	–	–	–	–	–
M12[a, b]	+	+	+	+	+	+	+	+	+	+	+	+	+	–	–
M13[c, d]	+	+	+	+	+	+	–	–	–	–	–	–	–	+	+
M15	–	–	–	–	–	+	–	–	–	–	–	–	–	–	–
M17[a, b]	+	+	+	+	–	+	+	+	+	+	+	+	+	–	–
M18[a, b]	+	+	+	+	+	+	+	+	+	+	+	+	+	–	–
M19[b, d]	+	+	+	–	–	–	–	–	–	–	–	–	–	–	–
M20[b]	+	+	+	+	+	+	–	–	–	–	–	–	–	–	–
M21[a, b]	+	+	+	–	–	–	+	+	+	+	+	+	+	–	–
M22[a, b]	+	+	+	–	–	–	+	+	+	+	+	+	+	–	–
M23[a, c, d]	+	+	+	–	–	–	+	+	+	+	+	+	+	+	+

RLM, MLM, and HLM represent rat, monkey, and human liver microsomes, respectively; RH, MH, and HH represent rat, monkey, and human hepatocytes, respectively.

+, metabolite detected; –, not detected.

[a] Metabolites formed in liver microsomes in the presence of NADPH-generating system.

[b] Metabolites formed in liver microsomes in the presence of NADPH-generating system and SAM.

[c] Metabolites formed in liver microsomes in the presence of UDPGA.

[d] Metabolites formed in liver microsomes in the presence of UDPGA and SAM.

DMD Fast Forward. Published on April 21, 2011 as DOI: 10.1124/dmd.111.038729
This article has not been copyedited and formatted. The final version may differ from this version.

Table 2 Identification of in vitro metabolites of rivoglitazone by LC-MS/MS.

Metabolite	Retention Time	$[M+H]^+$	Identity	Product Ions
	min	*m/z*		*m/z*
M6	16.1–16.2	402	TZD ring-opened methyl sulfoxide amide	161, 176 (B), 295, 321
M9	17.3–17.8	592	TZD ring-opened *N*-glucuronide	161, 176 (B), 282, 327, 373, 399, 416, 458
M10	18.1–18.6	418	TZD ring-opened methyl sulfone amide	161, 176 (B), 295, 321, 338
M11	18.9–19.1	464	*O*-Demethyl-*O*-sulfate	147, 162 (B), 242, 268, 384
M12	19.2–19.4	384	*O*-Demethyl rivoglitazone	147, 162 (B), 268, 313
M13	19.8	574	*N*-Glucuronide	161, 176 (B), 282, 398
M15	17.1	492	TZD ring-opened *S*-cysteine conjugate	161, 176 (B), 295, 340
M17	20.9–21.3	384	*N*-Demethyl rivoglitazone	147, 162 (B), 268, 313
M18	21.5–21.8	414	TZD ring 5-hydroxy rivoglitazone	161, 176 (B), 309, 354
M19	24.2–24.4	387	TZD ring-opened methylmercapto carboxylic acid	161, 176 (B), 282, 295
M20	20.4–20.9	386	TZD ring-opened methylmercapto amide	161, 176 (B), 281, 282, 294, 295
M21	16.3–16.6	356	TZD ring-opened hydroxy amide	161, 176 (B), 282, 311
M22	20.2	372	TZD ring-opened mercapto amide	161, 176 (B), 268, 282, 294, 327
M23	23.9	373	TZD ring-opened mercapto carboxylic acid	161, 176 (B), 268, 282, 295, 327

B, base peak.

Fig. 1

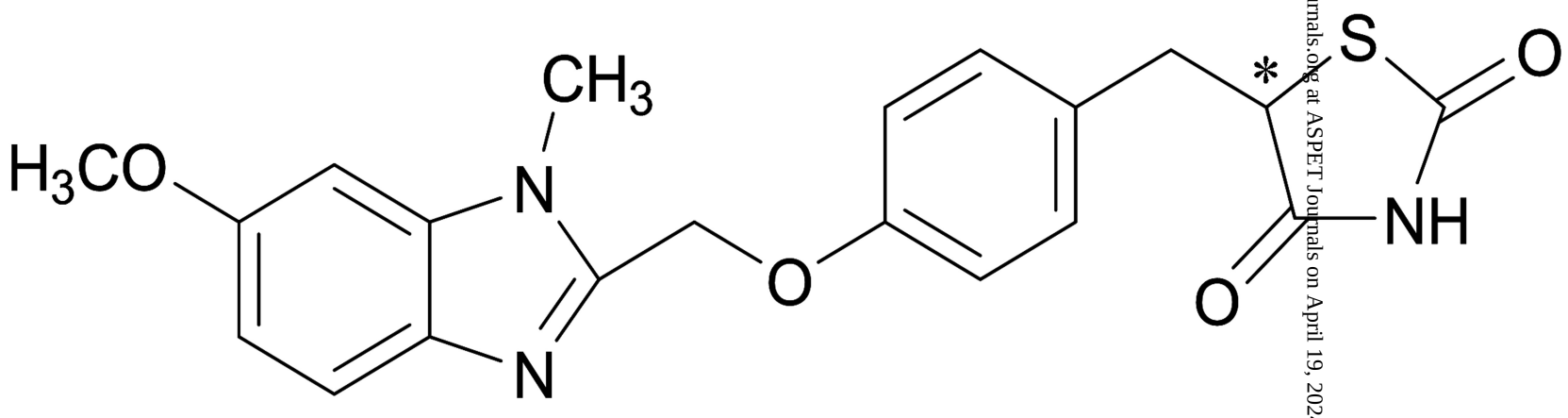

Rivoglitazone

Fig. 2

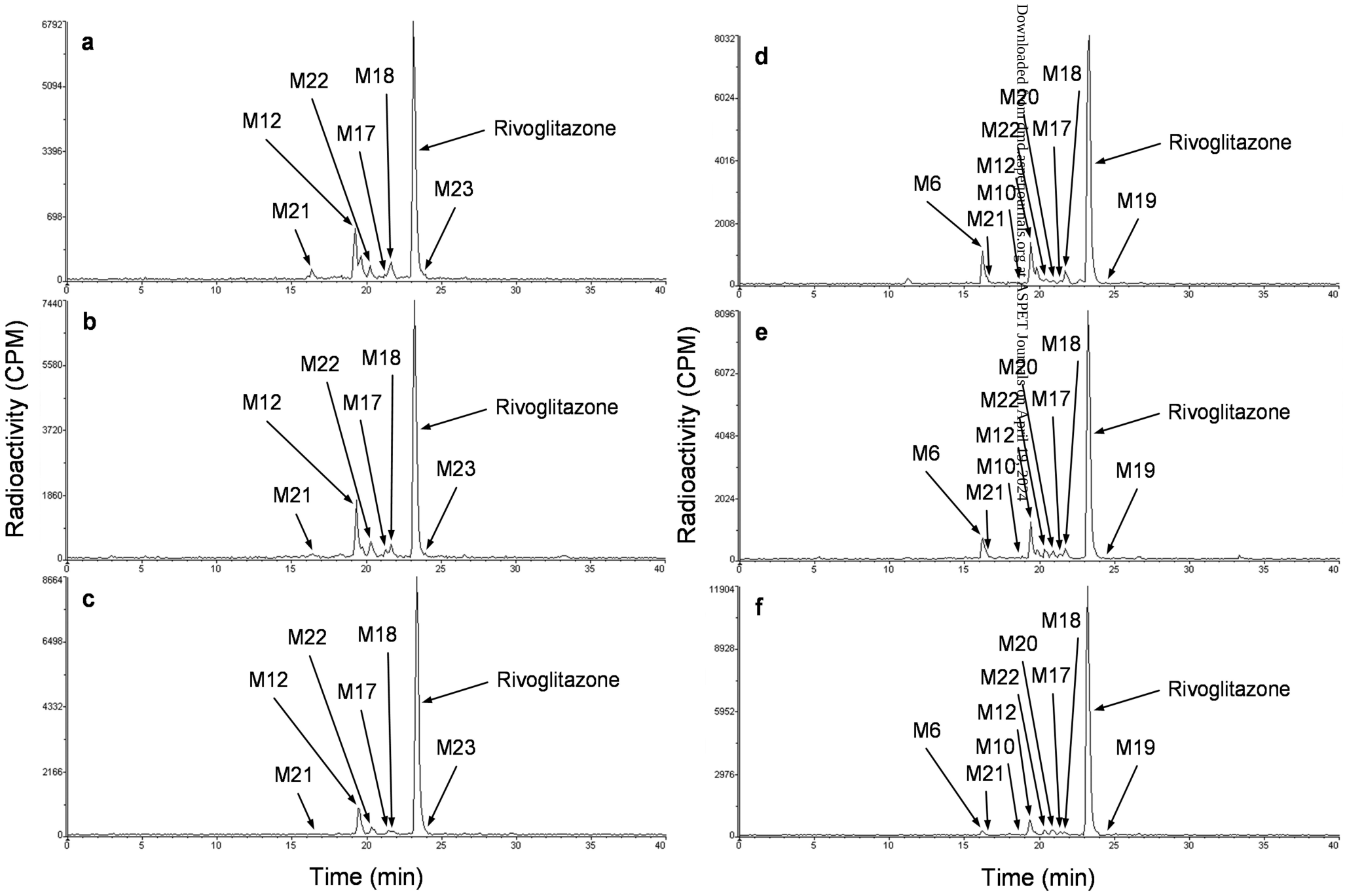

Fig. 3

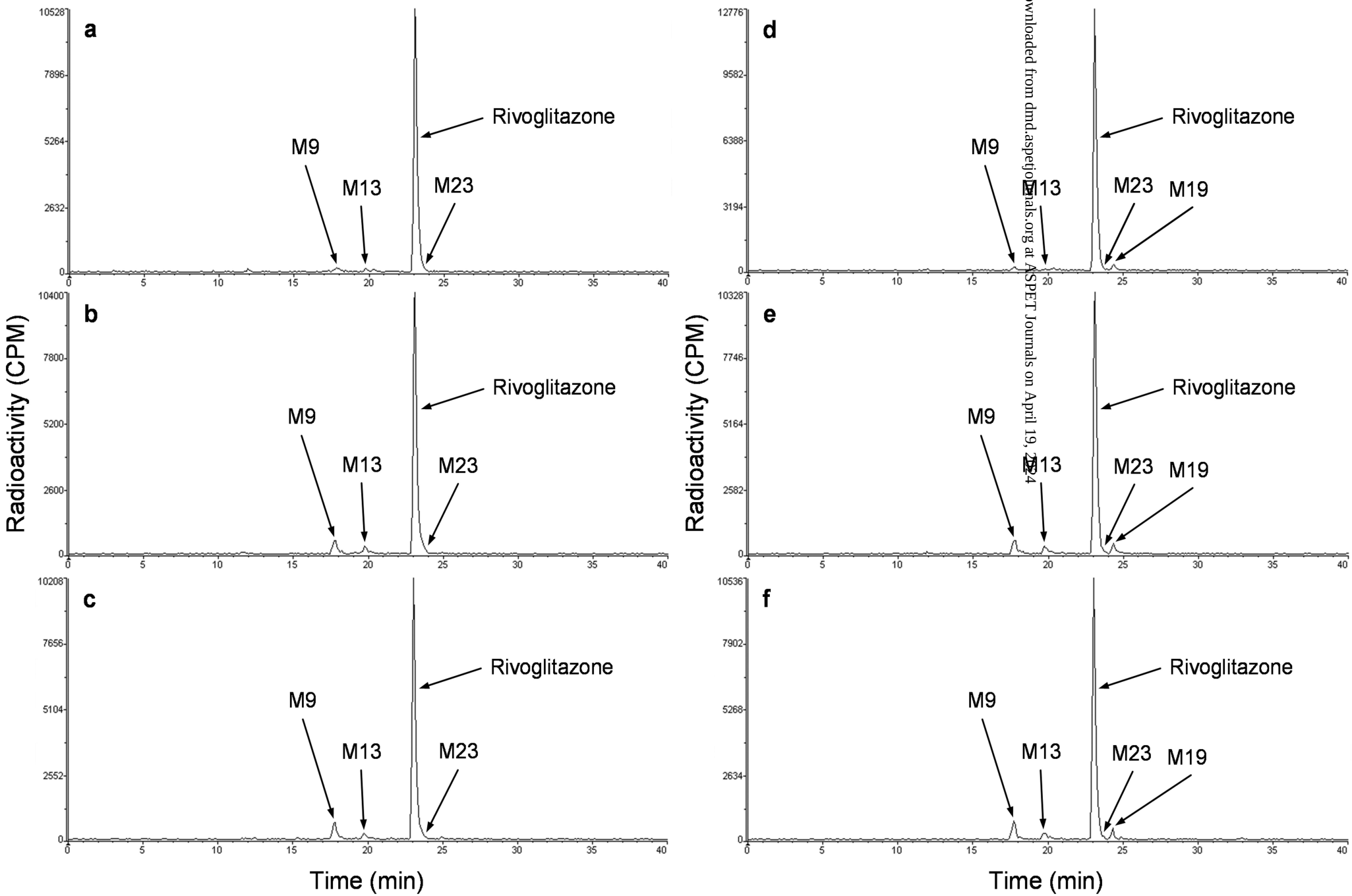

Fig. 4

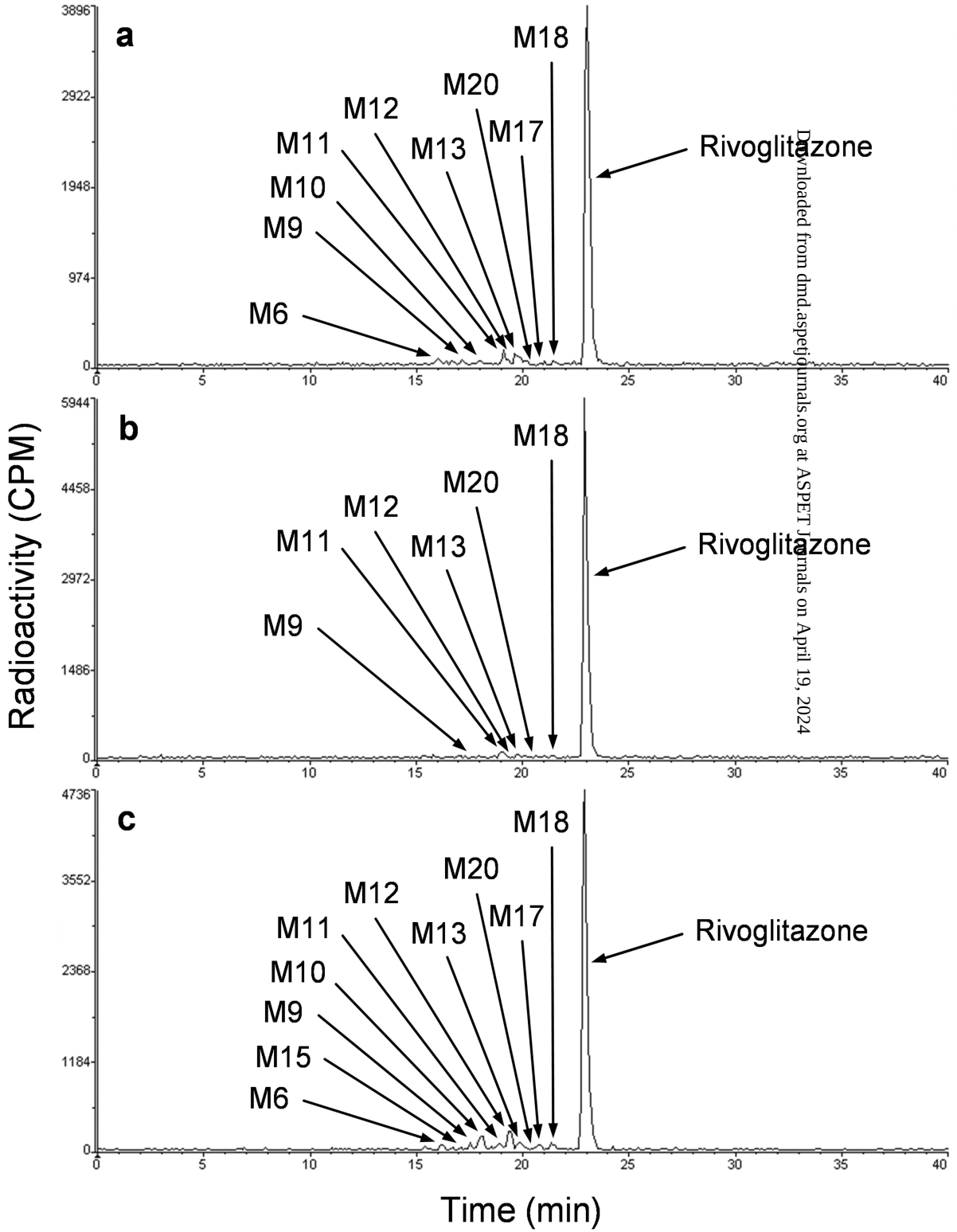

Fig. 5

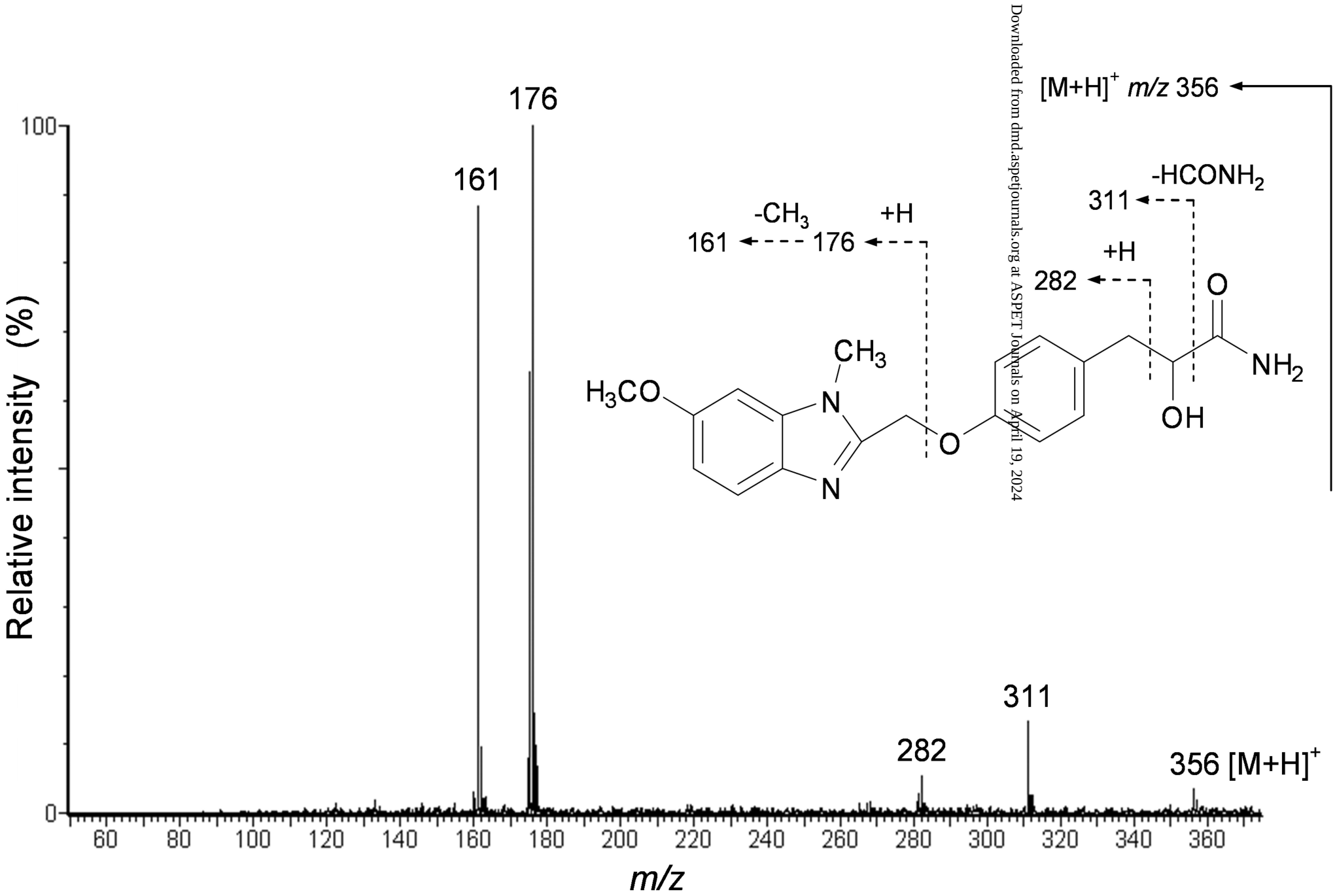

Fig. 6

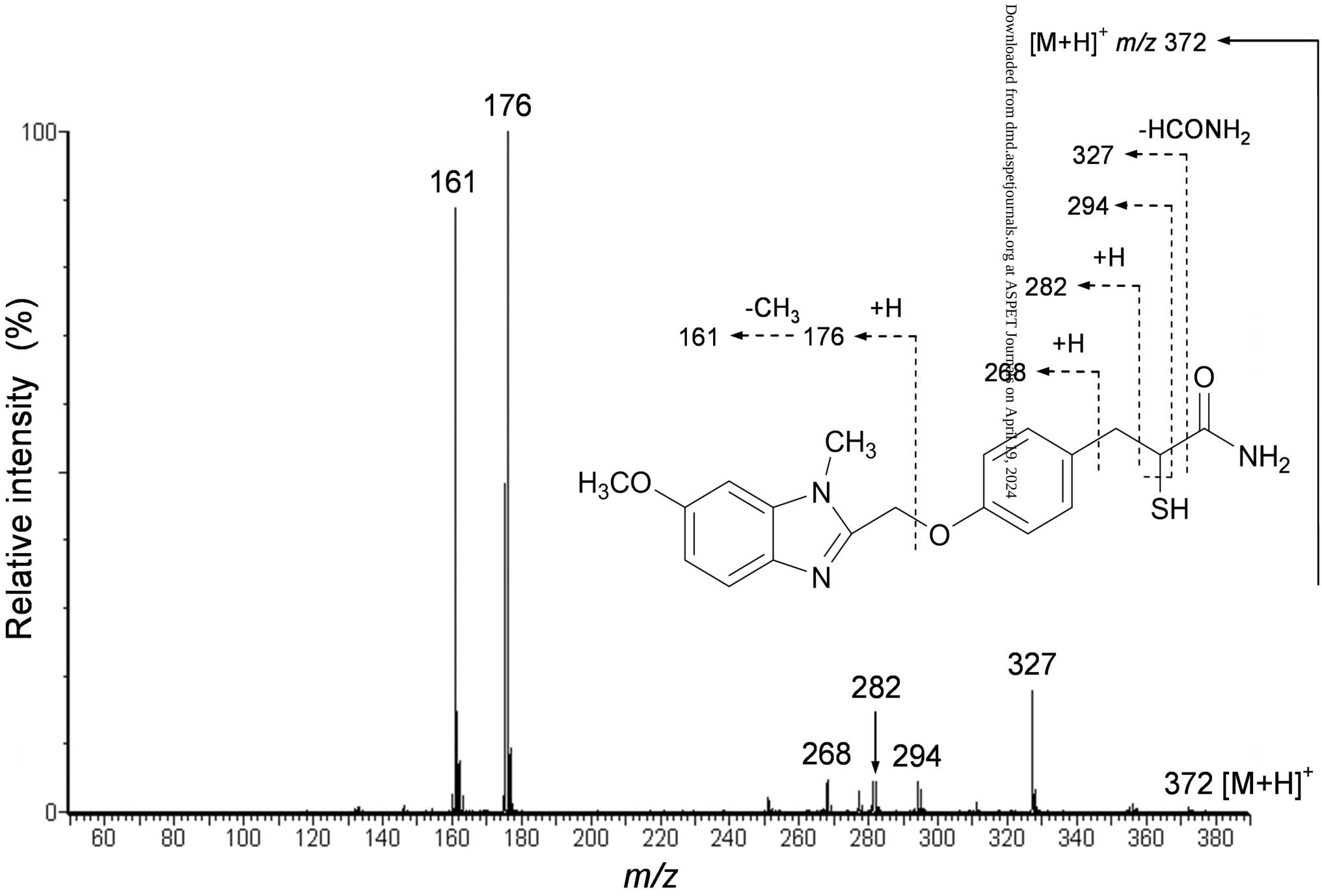

Fig. 7

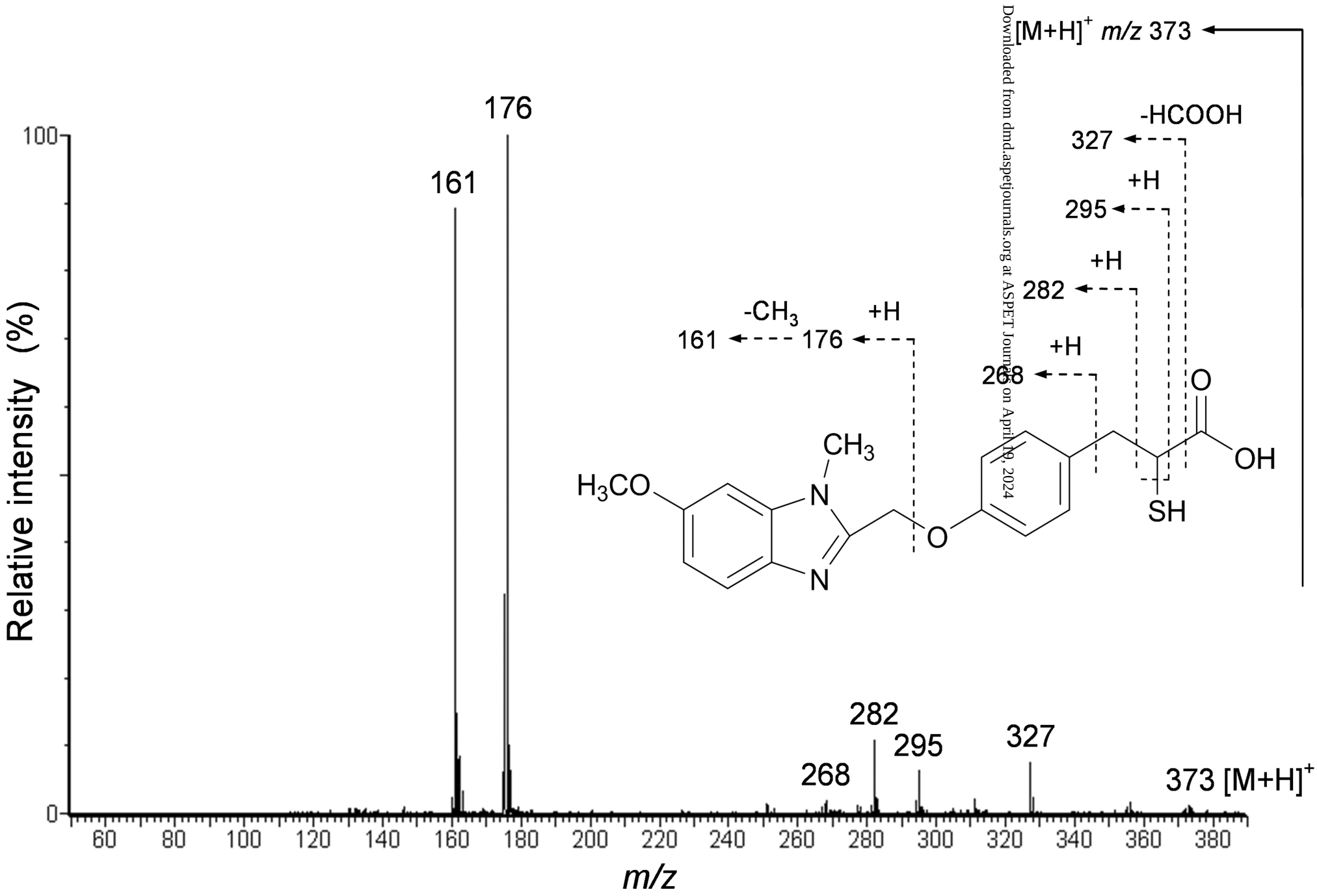

Fig. 8